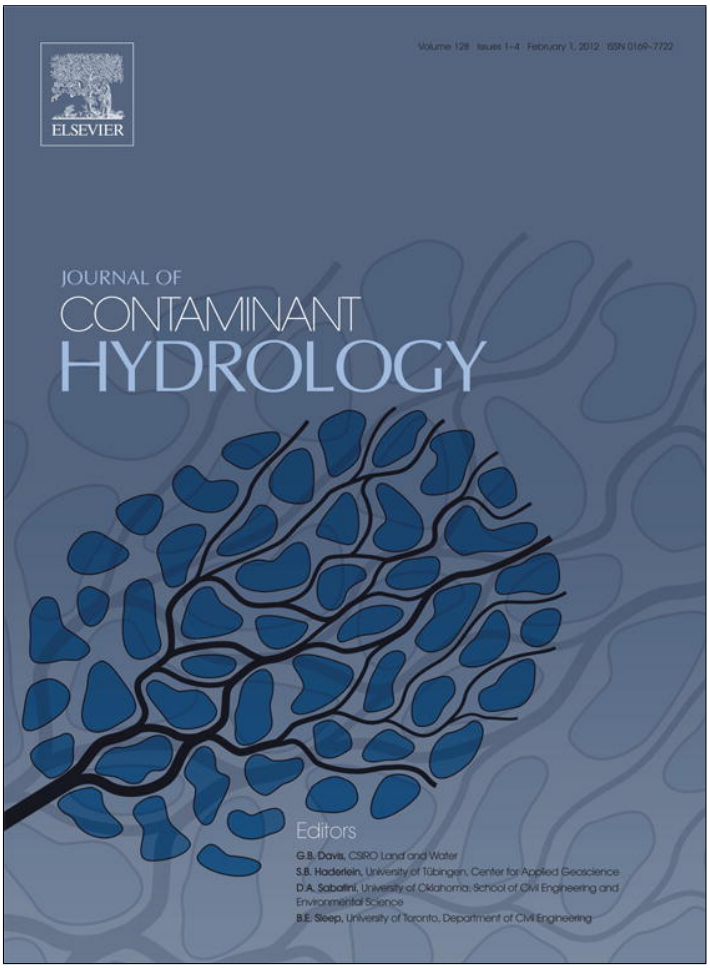

(This is a sample cover image for this issue. The actual cover is not yet available at this time.)

Journal of Contaminant Hydrology 133 (2012) 76–83

Contents lists available at SciVerse ScienceDirect

Journal of Contaminant Hydrology

journal homepage: www.elsevier.com/locate/jconhyd

Research article

Low pore connectivity in natural rock

Qinhong Hu [a,*], Robert P. Ewing [b], Stefan Dultz [c]

[a] Department of Earth and Environmental Sciences, The University of Texas at Arlington, 500 Yates Street, Box 19049, Arlington, TX 76019, United States
[b] Department of Agronomy, Iowa State University, 2104 Agronomy Hall, Ames, IA 50011, United States
[c] Institute of Mineralogy, Leibniz Universität Hannover, Callinstr. 3, D-30167 Hannover, Germany

ARTICLE INFO

Article history:
Received 2 July 2011
Received in revised form 14 March 2012
Accepted 15 March 2012
Available online 23 March 2012

Keywords:
Pore connectivity
Rock
Diffusion
Imbibition
Pore-scale network modeling

ABSTRACT

As repositories for CO_2 and radioactive waste, as oil and gas reservoirs, and as contaminated sites needing remediation, rock formations play a central role in energy and environmental management. The connectivity of the rock's porespace strongly affects fluid flow and solute transport. This work examines pore connectivity and its implications for fluid flow and chemical transport. Three experimental approaches (imbibition, tracer concentration profiles, and imaging) were used in combination with network modeling. In the imbibition results, three types of imbibition slope [log (cumulative imbibition) vs. log (imbibition time)] were found: the classical 0.5, plus 0.26, and 0.26 transitioning to 0.5. The imbibition slope of 0.26 seen in Indiana sandstone, metagraywacke, and Barnett shale indicates low pore connectivity, in contrast to the slope of 0.5 seen in the well-connected Berea sandstone. In the tracer profile work, rocks exhibited different distances to the plateau porosity, consistent with the pore connectivity from the imbibition tests. Injection of a molten metal into connected pore spaces, followed by 2-D imaging of the solidified alloy in polished thin sections, allowed direct assessment of pore structure and lateral connection in the rock samples. Pore-scale network modeling gave results consistent with measurements, confirming pore connectivity as the underlying cause of both anomalous behaviors: imbibition slope not having the classical value of 0.5, and accessible porosity being a function of distance from the edge. A poorly connected porespace will exhibit anomalous behavior in fluid flow and chemical transport, such as a lower imbibition slope (in air–water system) and diffusion rate than expected from classical behavior.

1. Introduction

Rock formations play a central role in energy, environmental, and water resources management, as oil and gas reservoirs, as repositories for CO_2 and radioactive waste, and as aquifers or contaminated sites needing remediation. Fluid flow and solute transport in rock are affected by the rock's porosity, permeability, tortuosity, and pore size distribution (Bear, 1972). These parameters are macroscopic consequences of the pore structure, which integrates geometry (e.g., pore size and shape, pore size distribution) and topology (e.g., pore connectivity) (Dullien, 1992). Sometimes topological factors outweigh the better-known geometrical factors (Ewing and Horton, 2002; Hu et al., 2002; Hunt, 2004), especially when the pore connectivity is low. However, the prevalence of low pore connectivity in rocks, and its impacts on fluid flow and chemical transport, are poorly documented and understood.

Many granular media, such as non-cemented sandstones, have a high coordination number (mean number of pores connected to a given pore). Others, such as crystalline rock or cemented sandstones, are less well connected. A network that is just barely connected is said to be at the percolation threshold, or at criticality (Stauffer and Aharony, 1994). Magma shrinks while cooling and crystallizing, generating internal stresses. Because the resulting fracture networks relieve stress when they reach the percolation threshold, crystalline rock porespaces are often near criticality (Guegen et al., 1991). For sedimentary rocks, Cook et al. (2011) reported that the diagenetic processes of compaction and cementation

* Corresponding author. Tel.: +1 817 272 5398; fax: +1 817 272 2628.
E-mail address: maxhu@uta.edu (Q. Hu).

0169-7722/$ – see front matter © 2012 Elsevier B.V. All rights reserved.
doi:10.1016/j.jconhyd.2012.03.006

(quartz overgrowths, and precipitation of potassium feldspar, illite, smectite, kaolinite, and calcite) will modify porosity, permeability and pore network architecture. Furthermore, Madden (1983), Mavko and Nur (1997), and Bernabé et al. (2010) reported that disconnection of the pore network usually occurs only at low (sometimes extremely low) porosities.

Fluid flow and solute transport in rock with low pore connectivity can be characterized by percolation theory (PT), the mathematics of flow pathways and scaling in disordered systems (Hunt and Ewing, 2009; Sahimi, 1994). Early adopted by researchers at Schlumberger (e.g., Koplik et al., 1988; Wilkinson, 1986), PT often suggests questions and interpretations of which more conventional approaches are unaware. For example, PT predicts that unsaturated hydraulic conductivity and solute diffusion may vanish at a non-zero water content θ_c, and that electrical conductivity σ will vary with proximity to that critical water content as $\sigma \sim (\theta - \theta_c)^2$ (Hunt and Ewing, 2009). In this paper, we use a percolation perspective to examine water imbibition and accessible porosity in rocks with different connectivities.

A property of particular relevance to low-connectivity porous media is that, at criticality, an increase in the size of the sample results in decreases in permeability, diffusivity, and accessible (similar to "effective") porosity, and an increase in tortuosity (Ewing and Horton, 2002; Stauffer and Aharony, 1994). A further complication is that, above but near the percolation threshold, there is some crossover length χ below which the system behaves anomalously, and above which it behaves classically. A consequence is that parameters of systems near or at criticality, measured in core-scale experiments, do not upscale trivially. Understanding the pore connectivity and quantifying this crossover length for a given rock are a key to correct upscaling.

Diffusion in systems near the percolation threshold is known to behave anomalously (Sahimi, 1994; Stauffer and Aharony, 1994), such that chemical travel times take on different spatial and temporal scaling (e.g., Ewing and Horton, 2002; Ewing et al., 2010). Matrix diffusion in fractured rock is recognized as important to the performance of geological repositories (i.e., Neretnieks, 1980), and to gas recovery from hydraulically-fractured shales (i.e., Bowker, 2007). Nonetheless, it is not widely appreciated that a rock's microscopic pore connectivity translates to macroscopic effects on fluid flow and chemical transport. This work assesses the pore connectivity in some rocks of interest to energy and environmental stewardship, compares different experimental approaches for assessing connectivity, and discusses implications of the low connectivity on fluid flow and chemical transport.

2. Materials and methods

2.1. Rock samples

Rocks studied in this work (Table 1) include sedimentary (sandstones, carbonate, and shale), igneous, and metamorphic types, and exhibit a range of porosity and permeability. The widely-studied Berea sandstone is un-cemented, macroscopically homogeneous, and has a narrow pore-size distribution; in contrast, cementation in the Indiana sandstone permits us to assess cementation effects on pore structure and connectivity. Likewise, diagenesis in carbonate rocks such as dolomite produces microporous grains and a wide range of pore sizes, resulting in a complex spatial distribution of pores and pore connectivity (Song et al., 2000). The welded tuff from Yucca Mountain has been intensively studied as a potential geological repository for high-level radioactive wastes, while the Barnett shale (currently the most productive gas field in the U.S.) is known for having extremely low gas diffusivity through its nm-size pores. The metagraywacke, a weakly metamorphosed sandstone characterized by irregular grain structure, is from a geothermal production site in northern California (Persoff and Hulen, 2001).

Table 1
Rock properties.

Rock	Source	Porosity (%)	Permeability (m^2)
Berea sandstone	Berea Quarry, OH	22.8	9.1×10^{-13}
Indiana sandstone	Gas Storage Formation, Lombard, IL	17.6	1.8×10^{-13}
Topopah Spring welded tuff	Yucca Mtn., NV	9.3	5.0×10^{-19}
Dolomite	Unknown	9.1	9.8×10^{-17}
Metagraywacke	The Geysers steam reservoir, CA	3.85	1.2×10^{-17}
Barnett shale	Gas reservoir, TX	1.27 ± 0.24 [a]	$(1–60)\times10^{-20}$ [b]

[a] Average ± standard deviation of six rectangular samples.
[b] Reported ranges from Sigal and Qin (2008).

2.2. Experimental and modeling approaches

2.2.1. Basic characterization

Helium porosity, and permeability to nitrogen gas, were measured for all rock core samples (2.54 cm i.d., 4 cm height) except the Barnett shale, by Core Laboratories Inc. (Aurora, CO) following standard methods in API RP 40 (1998). For the Barnett shale, porosity was determined by the method of Archimedes (Vennard and Street, 1975), weighing the sample (1) dried at 60 °C, (2) vacuum-saturated, and (3) saturated-and-submerged; this method measures the volume of all pores connected to the sample's exterior.

2.2.2. Water imbibition

Previous modeling work (Ewing and Horton, 2002) showed that pore connectivity could affect the progress of a diffusion front: rocks with well-connected porespace have the front advancing with the square root of time, while in rocks with sparsely-connected pores the front advances as approximately the one-fourth power of time. The imbibition test is a simple procedure for determining whether a rock sample has low pore connectivity, and for estimating the crossover length χ (depth to constant accessible porosity) in rocks. The test involves exposing one face of a rock sample to water, and measuring the mass of water uptake over time (Hu et al., 2001). Imbibition is mathematically analogous to diffusion in that, in classical homogeneous materials and if gravitational effects are negligible, the distance l to the wetting front increases with the square root of time: $l \sim t^{0.5}$ (Bruce and

Klute, 1956; Philip, 1957). If the accessible porosity is uniform with distance, then the cumulative mass of imbibed water I behaves identically: $I \sim t^{0.5}$. This relationship gives a slope of 0.5 in log space, which we call the imbibition slope. The imbibition test is faster than a diffusion test and requires less sophisticated equipment. Samples of different height-to-diameter ratios (i.e., shape) were tested to obtain additional information about the crossover length.

2.2.3. Accessible porosity profile

In a rock with sparsely-connected pores, the absolute porosity ϕ may be constant, but the porosity that is accessible from an edge (e.g., a fracture), ϕ_a, decreases with distance from that edge. Some of these accessible pores do not connect to the pore network that propagates across the whole rock. In percolation terminology, this "edge porosity", ϕ_e, is composed of finite pore clusters that happen to be intersected by the edge, in contrast to the "infinite cluster" which connects across arbitrary distances. Consequently, we expect ϕ_a to decrease with distance from the face until some distance χ, beyond which it stays constant. But if the rock has well-connected pores, χ is essentially zero, so ϕ_a is constant. Measuring ϕ_a as a function of distance from an edge therefore gives information about the rock's pore connectivity.

Rock samples were dried, subjected to vacuum, and then saturated with a solution containing both nonsorbing (bromide and perrhenate) and sorbing (cesium, cobalt, samarium, and strontium) tracers. A micro-scale laser (100 μm spot diameter, CETAC LSX-200 laser ablation system, CETAC Technologies, Omaha, NE) was then used to vaporize a hole into the rock sample in sub-micron depth increments, and the elements entrained in the vapor were analyzed with inductively coupled plasma-mass spectrometry (X-Series, Thermo Electron Corporation, West Palm Beach, FL). Successive laser pulses progressively deepened the hole. This laser ablation-inductively coupled plasma-mass spectrometry (LA-ICP-MS) approach has been used to directly map chemical distributions in rock at a spatial resolution of microns and a concentration limit of low-micrograms per gram (e.g., Hu and Möri, 2008). Because the tracers occupy only accessible pores and are not inherent to the rock samples, the resulting tracer concentration profiles give a direct measure of the accessible porosity profile.

2.2.4. Imaging of connected pore structures

Direct visualization is a compelling way to understand pore connectivity. 3-D micro-tomography approaches, including synchrotron-based light sources, have a spatial resolution down to a few microns, so 3-D visualization is usually limited to samples with large pores, such as sandstones (e.g., Fredrich et al., 2006). 2-D methods, while containing less overt information about connectivity, are capable of higher resolutions. Rock pore networks have been examined using Wood's metal (about 50% Bi, 25% Pb, 12.5% Zn and 12.5% Cd; melting point around 78 °C), a method pioneered by Swanson (1979) and Dullien (1981). Because of its high bismuth content, Wood's metal is not expected to shrink as it solidifies (Hildenbrand and Urai, 2003). Wood's metal injection also offers the possibility of freezing the invaded network at any stage of the injection, allowing micro-structural studies to be made on iteratively-filled pore networks (Kaufmann, 2009, 2010), although we did not do so in this study.

Our imaging method followed the method of Dultz et al. (2006). Dried cylindrical samples (a maximum size of 5 mm in diameter, 15 mm in length) were submerged in molten Wood's metal in a 100 °C autoclave. The autoclave was evacuated to <0.001 bar, then the molten alloy was forced into the accessible pores by applying an argon pressure of ~600 bar. At this pressure, with a surface tension of 0.4 N/m and a contact angle of 130° (Darot and Reuschle, 1999), Wood's metal intrudes pores with equivalent diameters as small as ~20 nm (Washburn, 1921). After the alloy solidified, 150 μm thick sections were polished and carbon-sputtered, then imaged with an environmental scanning electron microscope (Quanta 200, FEI, Hillsboro, OR) with back-scattered electrons. This method gives a high contrast between the light-colored Wood's metal-filled pores and the darker rock matrix.

2.2.5. Pore-scale network modeling

A pore-scale network model was developed to examine imbibition and accessible porosity as functions of pore connectivity. The model was validated against both analytical solutions and finite difference models at high connectivity, and against percolation scaling relationships at criticality (Ewing and Horton, 2002; Ewing et al., 2010). In essence, the model consists of a simple cubic lattice of sites connected by bonds, with the probability p of active bonds specified by the user, and the specification of which bonds are active determined pseudo-randomly. In the simple cubic lattice, the bond percolation threshold p_c is reached when bonds are active with a connection probability $p_c \approx 0.2488$ (Stauffer and Aharony, 1994). Simulations were run using multiple connection probabilities in the range $0.24 \le p \le 1.0$. The imbibition model releases random walkers at the inlet end of the network, and records their first arrival times at each distance (in lattice units) from the inlet. Because random walkers move as if by diffusion, at high connection probabilities the "wetting front" is expected to advance with the square root of time. The expected lower imbibition slope, at low pore connectivity, is $1/(2+(\mu-\beta)/\nu) \approx 0.263$, via the percolation exponents μ (≈ 2.0 in 3-D), β (≈ 0.41 in 3-D), and ν (≈ 0.88 in 3-D) (Stauffer and Aharony, 1994). Pore accessibility simulations used a lattice of size 1000^3, with 100 realizations. Imbibition simulations used a lattice of size 256^3, with 20 realizations and 250 random walkers per realization.

3. Results and discussion

3.1. Water imbibition

Imbibition experiments produced imbibition slopes from 0.2 to 0.5 (Fig. 1). For Berea sandstone, we observed the 0.5 slope across all the sample shapes, indicating well-connected pore spaces (Fig. 1a; Table 2). The larger slope of 0.649 shown for the shortest Berea sample (2 cm) is an artifact of initial sample settling, combined with the short time needed for the wetting front to reach the sample top; this gave relatively few data points to calculate the imbibition slope. The other Berea samples (e.g., Fig. 1a) also had high initial slope,

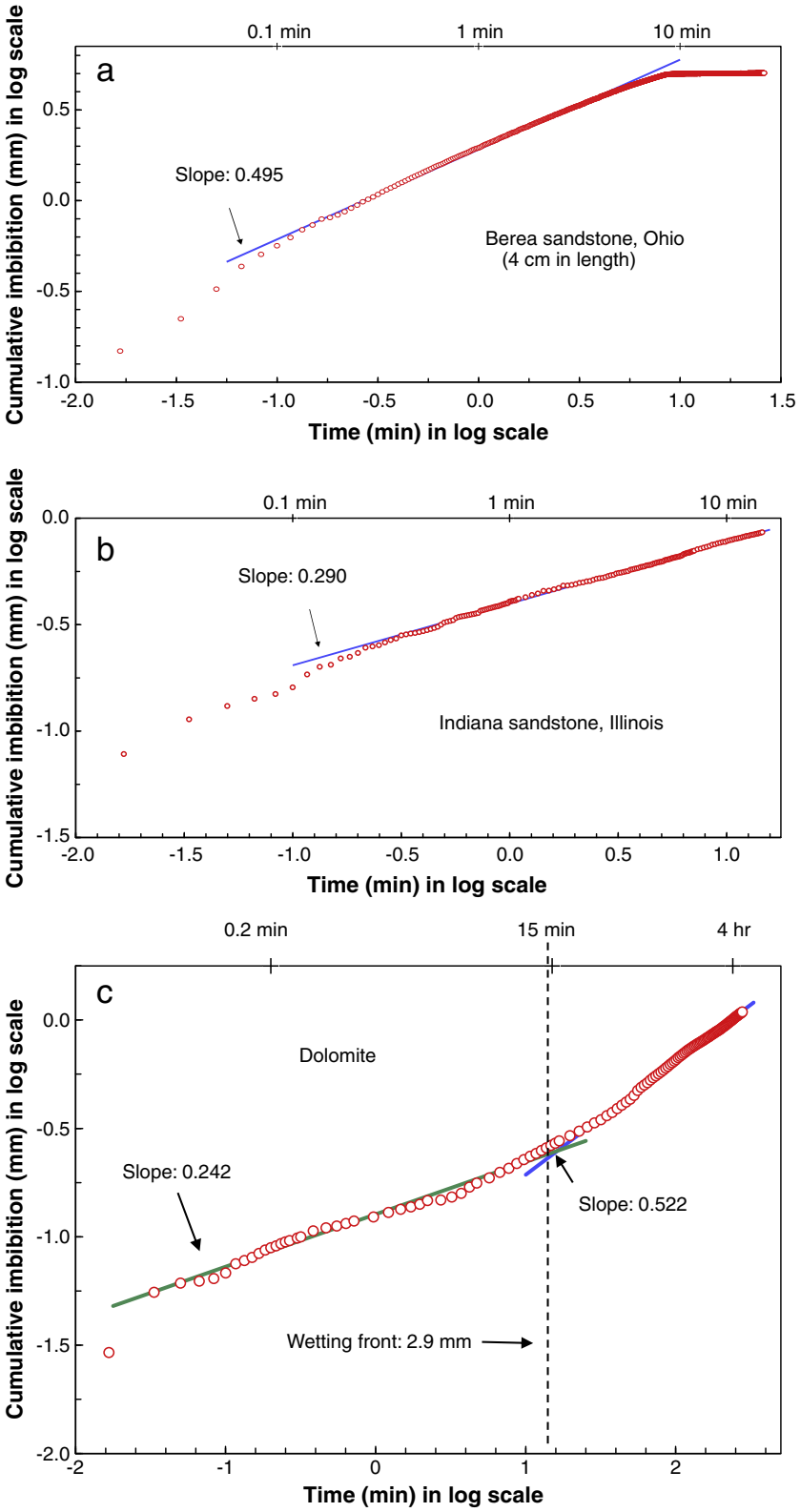

Fig. 1. Imbibition results for (a) Berea sandstone; the wetting front reaches the top of the 4 cm sample after about 10 min; (b) Indiana sandstone; and (c) dolomite. Y-axis in the figure is the cumulative imbibition, with the monitored water mass gain divided by the bottom area of the sample.

but imbibition proceeded for long enough that the fitted slope was not affected.

Although the cemented Indiana sandstone has porosity and permeability values similar to Berea sandstone, it consistently exhibited an imbibition slope around 0.26 (Fig. 1b; Table 2), indicating a lower pore connectivity than Berea sandstone. Poorly connected pore spaces were also evident in metagraywacke and Barnett shale: these samples have low porosity and nm-sized pore sizes, which tends to be associated with low pore connectivity.

Table 2
Behavior of imbibition slope related to sample shape.

Rock sample	Core diameter (cm)	Core height (cm)	Sample height/width	Imbibition slope[a]
Berea sandstone	1.7	2.0	1.18	0.649 ± 0.022
	1.7	4.0	2.35	0.488 ± 0.006
	1.7	8.0	4.71	0.494 ± 0.008
Indiana sandstone	5.0	2.0	0.40	0.272 ± 0.047
	1.5 (cube)	1.5 (cube)	1.00	0.301 ± 0.034
	1.7	2.0	1.16	0.268 ± 0.028
	1.7	4.0	2.33	0.293 ± 0.007
Welded tuff	5.0	2.0	0.40	0.513 ± 0.014
	1.5 (cube)	1.5 (cube)	1.00	0.366 ± 0.022
Dolomite	5.0	2.0	0.40	0.487 ± 0.035
	1.5 (cube)	1.5 (cube)	1.00	$\boldsymbol{0.268 \pm 0.041 \rightarrow 0.541 \pm 0.021}$[b]
	1.7	2.0	1.16	0.305 ± 0.024
	0.91	4.0	4.43	0.285 ± 0.037
Metagraywacke	5.0	2.0	0.40	0.277 ± 0.062
	1.5 (cube)	1.5 (cube)	1.00	0.267 ± 0.089
Barnett shale	1.4 (rectangular prism)	1.7 (rectangular prism)	1.12	0.267 ± 0.007

[a] Average ± standard deviation for at least triplicate measurements on the same core sample.
[b] Two-slope behavior as shown in Fig. 1c.

For the welded tuff and dolomite samples, imbibition slopes varied between 0.26 and 0.5, exhibiting intermediate pore connectivity. The slope value was related to the sample shape: tall thin samples were more likely to exhibit the 0.26 imbibition slope, perhaps later crossing over to 0.5-type behavior, while short, squat samples were more likely to have a slope of 0.5 (Table 2). With a sample shape factor of 1.0, dolomite imbibition initially proceeded as $I \sim t^{0.26}$, and then switched to classical ($t^{0.5}$) behavior (Fig. 1c). The distance to the wetting front at which the slope changed is the crossover length χ of percolation theory. Assuming that accessible porosity varies as discussed in Section 3.2, we calculated $\chi \approx 2.05$ mm for the dolomite sample (Fig. 1c).

Simulations likewise give an imbibition slope of 0.5 at high pore connectivity ($p > 0.28$), and 0.26 at $p = p_c$ (the percolation threshold). At intermediate values (say, $p \approx 0.25$), the slope transitions from 0.26 to 0.5 after some finite imbibition time (Fig. 2). In other words, just above the percolation threshold, water imbibition (analogous to solute diffusion) is anomalous at short times and distances, but later assumes "classical" (Fickian) long-term behavior. Consistent with percolation theory and pore-scale network modeling, this work with different types of rock shows that anomalous behavior (slope of 0.26) is observed at some scales and classical at

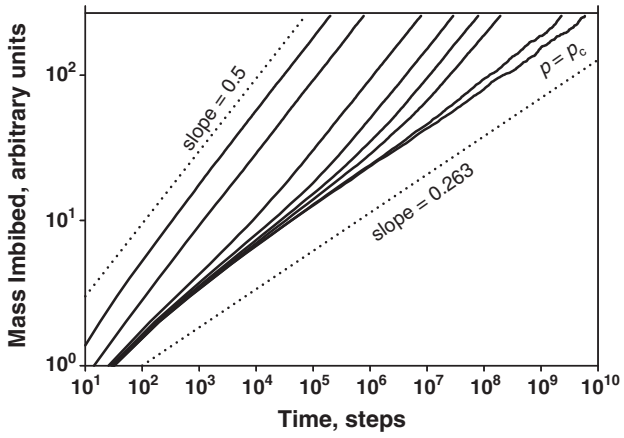

Fig. 2. Pore-scale network modeling results of imbibition for rocks with different pore connectivity. Solid lines correspond to connection probabilities (from left to right) $p = 1.0, 0.5, 0.3, 0.27, 0.26, 0.255, 0.25$, and p_c (≈ 0.2488).

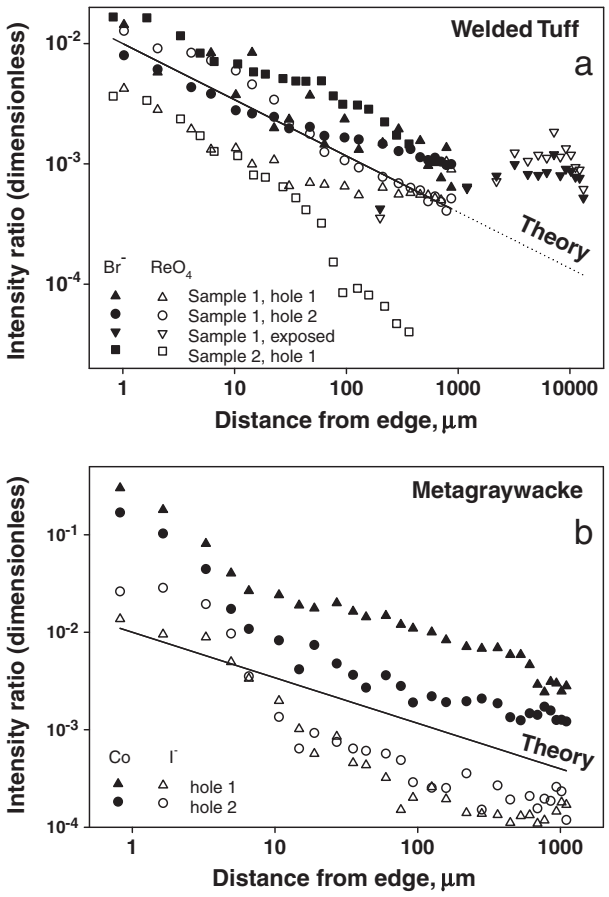

Fig. 3. Tracer-occupied connected pore spaces after vacuum-saturation and LA-ICP-MS depth mapping; intensity ratios on the Y-axis are the division of ICP-MS signal intensity (in counts per second) for tracer to the intensity for an intrinsic element in the rock (aluminum Al). (a) Results of welded tuff with Br^- and ReO_4^- as non-sorbing tracers; A and B are two locations with depth mapping. (b) Results of metagraywacke with Co^{2+} and I^-.

others (Table 2). Additionally, making a lattice taller and thinner (not shown) has a similar effect on the imbibition slope as decreasing the connection probability p.

3.2. Accessible porosity

The concentration of tracers with depth (Fig. 3) decreases linearly in log–log space, then (in most samples) becomes constant. The change in slope of the concentration profile (when present) occurs at χ, the effective depth of the edge porosity. In welded tuff, the plateau is around 300 μm deep (Fig. 3a). In metagraywacke, it appears that the plateau was not reached even at the maximum sampled depth of 850 μm (Fig. 3b). This is consistent with the imbibition measurements (Table 2), which indicate lower pore connectivity in metagraywacke than in welded tuff.

Percolation theory gives an accessible porosity varying with distance l, for $l<\chi$, as $\phi_a \sim l^{-\beta/\nu}$, using the exponents β and ν mentioned in Section 2.2.5. The shape of the measured concentration profile for both welded tuff and metagraywacke matches the pore-scale network simulations with different pore connectivities (Fig. 4) and the theoretical slope of $-\beta/\nu$, indicating that pore connectivity suffices to explain the observed increase in near-edge accessible porosity.

The porosity of welded tuff is approximately 9% (Table 1), and nearly all the pores are smaller than 1 μm in diameter, as given by our water absorption isotherm measurements (not shown). Assuming a mean pore size of 1 μm gives a unit cell size on the order of 2.16 μm. The observed correlation length $\chi \approx 300$ μm (Fig. 3a) then corresponds to about 140 pores, which is similar to the network results for connectivity $p=0.25$. We might therefore expect the welded tuff to behave like a $p=0.25$ network for imbibition (Fig. 2), and in fact we get 0.26-type behavior when the tuff core's shape factor is 1.0, and only see a slope of 0.5 when the sample is short and squat (Table 2). This illustrates the synergy between experimental and modeling approaches in understanding core-scale behavior caused by pore-scale phenomena.

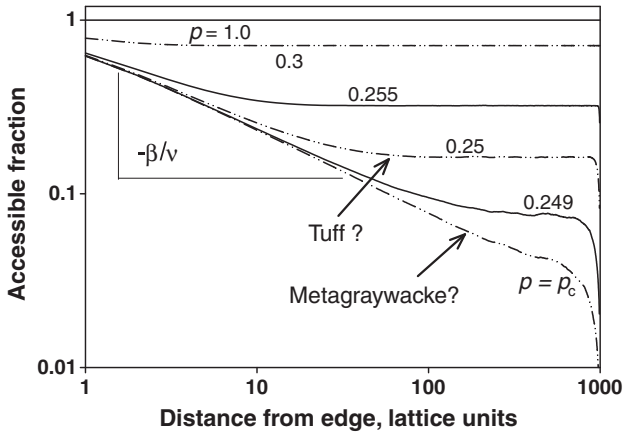

Fig. 4. Pore-scale network modeling results for accessible-porosity distribution for rocks with different pore connectivity. Connectivities analogous to welded tuff and metagraywacke are indicated on the figure.

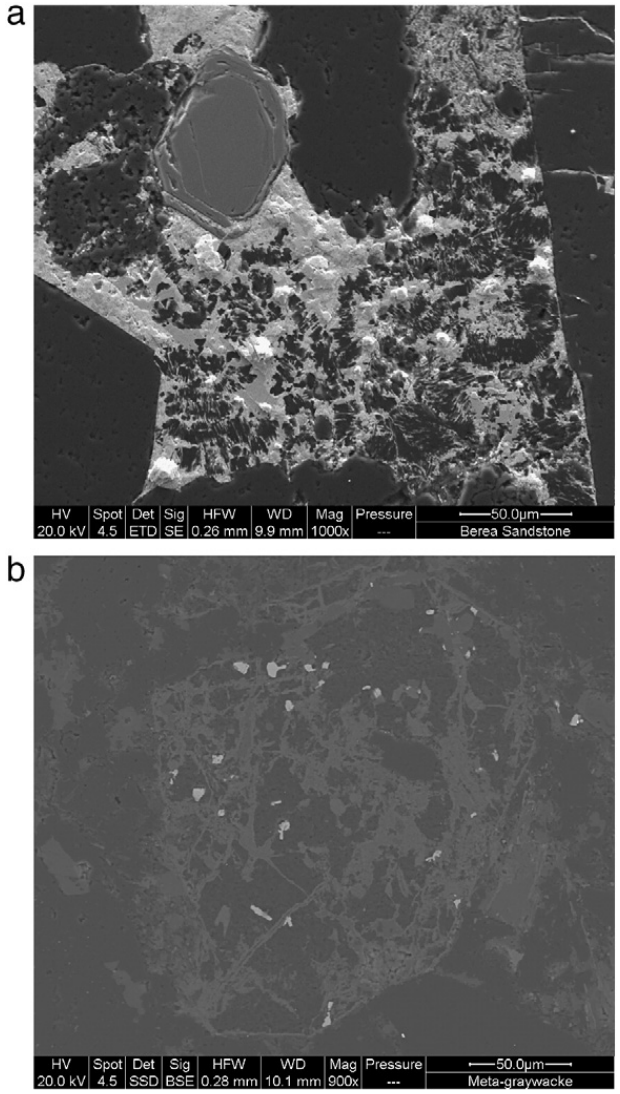

Fig. 5. SEM-BSE images of connective pores occupied by the alloy Wood's metal (bright graytone) in (a) well-connected Berea sandstone; and (2) poorly-connected metagraywacke. Pores (bottle-necked or isolated) not intruded by Wood's metal in the samples appear black. The images were taken at similar magnifications (1000× for Berea sandstone and 900× for metagraywacke), with the scale bar of 50 μm indicated on the images.

3.3. Pore connection from injection of a molten alloy

Five of the six rocks examined in this study were injected with Wood's metal and then imaged. The pressures available (600 bar) can't interrogate the pore system in the Barnett shale, which has a reported mean pore diameter of only 5 nm (Bowker, 2007). Fig. 5 shows examples of SEM-Back Scattered Electron images taken for Wood's metal-injected Berea sandstone and metagraywacke under similar magnifications. Although these 2-D images do not provide a direct view of 3-D pore connectivity, some assessments of pore size, pore geometry, and lateral connection can be garnered from the sharp contrast between Wood's metal-occupied pore spaces and the rock matrix. Berea sandstone has many μm-sized pores (Fig. 5a) that are better connected than the much smaller, more isolated pores in metagraywacke (Fig. 5b). This is consistent with the results from both imbibition tests and tracer-concentration profiles, indicating that

Berea sandstone pores are well-connected while those in metagraywacke are not. For the Berea sandstone, our water absorption isotherm results indicate that 90% of the pores (by volume) are smaller than 200 μm (this was confirmed by computed tomography imaging with a spatial resolution of 12 μm), but only 20% are smaller than 0.3 μm. In contrast, metagraywacke has 90% pores smaller than 20 nm, and 20% smaller than about 2 nm (Persoff and Hulen, 2001). The Wood's metal approach provides a direct visual corroboration of pore size and lateral connection; serial sectioning and image analysis would make this approach quantitative.

4. Conclusion

Using complementary core-scale measurements and pore-scale network modeling, this work reports a high prevalence of low pore connectivity in natural rock, from processes such as diagenesis (cementation in Indiana sandstone) and metamorphism (metagraywacke). Examining rocks with different porosity and permeability values, we illustrate the utility and complementarity of our experimental approaches in combination with pore-scale network modeling. Consistently across approaches, we found well-connected pores for Berea sandstone, intermediately-connected pores in welded tuff and dolomite, and a sparsely-connected pore system for Indiana sandstone, metagraywacke, and Barnett shale. Low pore connectivity, such as detected with the methods described here, is expected to further manifest itself in anomalous fluid flow and chemical transport, such as a diffusion rates deviating from classical behavior.

The imbibition tests indicated a crossover length in dolomite of about 2.0 mm. Micro-scale mapping using LA-ICP-MS of accessible pore spaces gave crossover lengths of about 300 μm for welded tuff, and perhaps 1 mm for metagraywacke. Considering the complex pore structure in natural rock, such as the nm-sized pore spaces in shale samples, other techniques (such as nm-scale focused ion beam/SEM and small-angle neutron scattering imaging) would further enhance our ability to examine pore connectivity and its emergent consequences for fluid flow and chemical transport.

Acknowledgments

Funding for this project is partly provided by the University of Texas at Arlington, and RPSEA through the "Ultra-Deepwater and Unconventional Natural Gas and Other Petroleum Resources" program authorized by the U.S. Energy Policy Act of 2005. RPSEA (www.rpsea.org) is a nonprofit corporation whose mission is to provide a stewardship role in ensuring the focused research, development and deployment of safe and environmentally responsible technology that can effectively deliver hydrocarbons from domestic resources to the citizens of the United States. RPSEA, operating as a consortium of premier U.S. energy research universities, industry, and independent research organizations, manages the program under a contract with the U.S. Department of Energy's National Energy Technology Laboratory. A portion of the research was performed using EMSL, a national scientific user facility sponsored by the Department of Energy's Office of Biological and Environmental Research and located at Pacific Northwest National Laboratory (PNNL). PNNL is operated for DOE by Battelle under contract DE-AC06-76RLO 1830. The views and opinions of authors expressed herein do not necessarily state or reflect those of the United States Government or any agency thereof.

References

American Petroleum Institute Recommended Practice (API RP) 40, Recommended Practice for Core Analysis Procedure, 2nd ed. Am. Petrol. Inst, Washington, DC.
Bear, J., 1972. Dynamics of Fluid in Porous Media. Dover, New York.
Bernabé, Y., Li, M., Maineult, A., 2010. Permeability and pore connectivity: a new model based on network simulations. Journal of Geophysical Research 115 (B10), B10203.
Bowker, K.A., 2007. Barnett shale gas production, Fort Worth Basin: issues and discussion. AAPG Bulletin 91 (4), 523–533.
Bruce, R.R., Klute, A., 1956. The measurement of soil–water diffusivity. Soil Science Society of America Proceedings 20, 458–462.
Cook, J.E., Goodwin, L.B., Boutt, D.F., 2011. Systematic diagenetic changes in the grain-scale morphology and permeability of a quartz-cemented quartz arenite. AAPG Bulletin 95 (6), 1067–1088.
Darot, M., Reuschle, T., 1999. Direct assessment of Wood's metal wettability on quartz. Pure and Applied Geophysics 155 (1), 119–129.
Dullien, F.A.L., 1981. Wood's metal porosimetry and its relation to mercury porosimetry. Powder Technology 29, 109–116.
Dullien, F.A.L., 1992. Porous Media: Fluid Transport and Pore Structure2nd ed. Academic Press, San Diego.
Dultz, S., Behrens, H., Simonyan, A., Kahr, G., Rath, T., 2006. Determination of porosity and pore connectivity in feldspars from soils of granite and saprolite. Soil Science 171 (9), 675–694.
Ewing, R.P., Horton, R., 2002. Diffusion in sparsely connected pore spaces: temporal and spatial scaling. Water Resources Research 38 (12), 1285. doi:10.1029/2002WR001412.
Ewing, R.P., Hu, Q.H., Liu, C.X., 2010. Scale dependence of intra-granular porosity, diffusivity, and tortuosity. Water Resources Research 46, W06513. doi:10.1029/2009WR008183.
Fredrich, J.T., Digiovanni, A.A., Noble, D.R., 2006. Predicting macroscopic transport properties using microscopic image data. Journal of Geophysical Research, Solid Earth 111 (B3). doi:10.1029/2005jb003774.
Guegen, Y., David, C., Gavrilenko, P., 1991. Percolation networks and fluid transport in the crust. Geophysics Review and Letters 18, 931–934.
Hildenbrand, A., Urai, J.L., 2003. Investigation of the morphology of pore space in mudstones — first results. Marine Petroleum Geology 20 (10), 1185–1200.
Hu, Q., Möri, A., 2008. Radionuclide transport in fracture-granite interface zones. Physics and Chemistry of the Earth 33 (14–16), 1042–1049.
Hu, Q., Persoff, P., Wang, J.S.Y., 2001. Laboratory measurement of water imbibition into low-permeability welded tuff. Journal of Hydrology 242 (1–2), 64–78.
Hu, Q., Kneafsey, T.J., Trautz, R.C., Wang, J.S.Y., 2002. Tracer penetration into welded tuff matrix from flowing fractures. Vadose Zone Journal 1, 102–112.
Hunt, A.G., 2004. Percolative transport and fractal porous media. Chaos Solitons Fractals 19, 309–325.
Hunt, A.G., Ewing, R.P., 2009. Percolation theory for flow in porous media. Lect. Notes Phys., 771. Springer, Berlin.
Kaufmann, J., 2009. Characterization of pore space of cement-based materials by combined mercury and Wood's metal intrusion. Journal of the American Ceramic Society 92 (1), 209–216.
Kaufmann, J., 2010. Pore space analysis of cement-based materials by combined nitrogen sorption — Wood's metal impregnation and multi-cycle mercury intrusion. Cement Concrete Comparative 32 (7), 514–522.
Koplik, J., Redner, S., Wilkinson, D., 1988. Transport and dispersion in random networks with percolation disorder. Physical Review A: Mathematical and General 37, 2619–2636.
Madden, T.R., 1983. Microcrack connectivity in rocks: a renormalization group approach to the critical phenomena of conduction and failure in crystalline rocks. Journal of Geophysical Research 88 (B1), 585–592.
Mavko, G., Nur, A., 1997. The effect of a percolation threshold in the Kozeny–Carman relation. Geophysics 62, 1480–1482.
Neretnieks, I., 1980. Diffusion in the rock matrix: an important factor in radionuclide retardation? Journal of Geophysical Research 85, 4379–4397.
Persoff, P., Hulen, J.B., 2001. Hydrologic characterization of reservoir metagraywacke from shallow and deep levels of the Geysers vapor-dominated geothermal system, California. Geothermal 30, 169–192.
Philip, J.R., 1957. The theory of infiltration: 4. Sorptivity and algebraic infiltration equations. Soil Science 84, 257–265.

Sahimi, M., 1994. Applications of Percolation Theory. Taylor and Francis, London.
Sigal, R.F., Qin, B., 2008. Examination of the importance of self diffusion in the transportation of gas in shale gas reservoirs. Petrophysical 49 (3), 301–305.
Song, Y.Q., Ryu, S.G., Sen, P.N., 2000. Determining multiple length scales in rocks. Nature 406 (6792), 178–181.
Stauffer, D., Aharony, A., 1994. Introduction to Percolation Theory, 2nd ed. Taylor and Francis, London.
Swanson, B.F., 1979. Visualizing pores and nonwetting phase in porous rock. Journal of Petroleum Technology 31, 10–18.
Vennard, J.K., Street, R.L., 1975. Elementary Fluid Mechanics. John Wiley and Sons, Inc, New York.
Washburn, E.W., 1921. Note on a method of determining the distribution of pore sizes in a porous materials. Proceedings of the National Academy of Sciences 7, 115–116.
Wilkinson, D., 1986. Percolation effects in immiscible displacement. Physical Review A 34, 380–391.